WPDA: Frequency-based Backdoor Attack with Wavelet Packet Decomposition

Zhengyao Song, Yongqiang Li, Danni Yuan, Li Liu, Shaokui Wei and Baoyuan Wu

Abstract—This work explores an emerging security threat against deep neural networks (DNNs) based image classification, i.e., backdoor attack. In this scenario, the attacker aims to inject a backdoor into the model by manipulating training data, such that the backdoor could be activated by a particular trigger and bootstraps the model to make a target prediction at inference. Currently, most existing data poisoning-based attacks struggle to achieve success at low poisoning ratios, increasing the risk of being defended by defense methods. In this paper, we propose a novel frequency-based backdoor attack via Wavelet Packet Decomposition (WPD), WPD decomposes the original image signal to a spectrogram that contains frequency information with different semantic meanings. We leverage WPD to statistically analyze the frequency distribution of the dataset to infer the key frequency regions the DNNs would focus on, and the trigger information is only injected into the key frequency regions. Our method mainly includes three parts: 1) the selection of the poisoning frequency regions in spectrogram; 2) trigger generation; 3) the generation of the poisoned dataset. Our method is stealthy and precise, evidenced by the 98.12% Attack Success Rate (ASR) on CIFAR-10 with the extremely low poisoning ratio 0.004% (i.e., only 2 poisoned samples among 50,000 training samples) and can bypass most existing defense methods. Besides, we also provide visualization analyses to explain why our method

Index Terms—Backdoor attack, wavelet packet transform, low poisoning ratios

I. INTRODUCTION

DEEP neural networks (DNNs) have been widely used in various research fields with great success (e.g., face recognition [3], [10], voice recognition [26], [56], and autonomous driving [62]), which provide intelligence for human life, but also bring many security risks. One of the typical security threats is the backdoor attack, which can make a trained DNN model performs specific behaviors when encountering a particular trigger pattern, while not affecting the performance of benign samples.

In this work, we study the threat model of data poisoningbased backdoor attack, where the attack can only manipulate the training dataset, without access to the training process. It applies to the practical scenario that the user doesn't have sufficient training data, thus download or buy data from

Zhengyao Song and Yongqiang Li are with School of Instrumentation Science and Engineering, Harbin Institute of Technology, Harbin, China, e-mail: songzhengyao@stu.hit.edu.cn, liyongqiang@hit.edu.cn.

Danni Yuan, Shaokui Wei and Baoyuan Wu are with the School of Data Science, The Chinese University of Hong Kong, Shenzhen, China, email: danniyuan@link.cuhk.edu.cn, shaokuiwei@link.cuhk.edu.cn, wubaoyuan@cuhk.edu.cn.

Li Liu is with the Hong Kong University of Science and Technology (Guangzhou), China, email: avrillliu@hkust-gz.edu.cn.

Corresponding Author(s): Yongqiang Li and Baoyuan Wu.

an untrustworthy third-party data platform. Although several effective backdoor attacks have been developed, they often require a substantial poisoned training samples to achieve the desired attack success rate, potentially increasing the risk of being defend by defense methods. Our goal is to achieve a stealthy and stable attack at low poisoning ratios, which is necessary and challenging [50].

The poisoned samples generated by spatial domain-based backdoor attacks, which can achieve success at low poisoning ratios, usually tend to have anomalous pixels. To tackle this issue, we propose to explore in the frequency domain. Frequency-domain-based backdoor attacks can perform more granular manipulations on specific parts of the image, and it is also easier to maintain the naturalness of the image. Currently, several techniques exist for transforming an image from spatial space to frequency space, including the Discrete Cosine Transform (DCT) [1], Discrete Fourier Transform (DFT) [49], and Wavelet Packet Decomposition (WPD) [54]. Among these methods, WPD can provide a unique multi-scale frequency domain analyses. This capability enables WPD to effectively capture features at various scales within an image, thereby enhancing the overall understanding of the image's structural composition. Furthermore, WPD excels in accurately locating and representing local features with different semantic meanings of the image in the frequency domain. With the aim of proposing a precise and stable attack method, we leverage the capability of WPD to selectively modify the key frequency regions in the spectrogram based on the distribution of frequency information in the dataset. We also conduct qualitative analyses to improve the trigger to promote the model to learn the trigger information more effectively. Additionally, we offer visualization analyses based on l_2 -distance Kernel Density Estimation (KDE) to explain the reasons for the effectiveness of our method at low poisoning ratios.

The main contributions of this work includes the following four aspects:

- We explore the frequency distribution of different datasets by WPD to infer which frequency regions the NNs would focus on.
- We propose a data-poisoning based attack method, denoted as WPDA, which can achieve a desired ASR even at extremely low poisoning ratios.
- Comprehensive experimental evaluations show the superior results of our method, especially at the low poisoning ratios. Besides, extensive qualitative analyses reveal the reasons for the effectiveness of WPDA.
- We provide l₂-distance Kernel Density Estimation (KDE) visualization analyses to explain why our method works

and demonstrate that our method promotes the model effectively learn the trigger rather than memorizing the poisoned training samples.

Organization. The structure of the remainder of the paper is outlined as follows: In Section II , we provide a comprehensive review of related work pertaining to backdoor attacks and defenses. Following this, we introduce the preliminary theory of the wavelet packet transform and define the problem formulation. We describe the implementation of our method in detail in Section III. In Section IV, We compare our method with 7 SOTA attack methods in terms of attack performance and defense performance. In Section V, we conduct t-SNE and l_2 -distance KDE visualization experiments to analyze our method and other attacks. Finally, we conclude our work in Section VI.

II. RELATED WORK

A. Backdoor Attack

Current research about backdoor attacks can be interpreted as the process of maliciously implanting a backdoor into the model, which would induce the model to build the relationship between special input triggers with a desired output. The main methodologies include poisoning training data [8], [15], [18], [29], [37], [60], manipulating the model's parameters [24], [43], or controlling the training process [2], [12], [32], [33], [38]. In particular, attackers can manipulate both images and labels [8], [18], [29] in data poisoning works.

BadNets [18] is a pioneering work on backdoor attacks in image classification tasks that injects a white patch into benign samples. Following this, lots of backdoor attack are proposed, such as Blended [8], which takes a cartoon image as the trigger and blends it with the benign samples. Li et al. [8] propose a reflection backdoor attack, which enhances backdoor attack by applying random spatial transformations to the poisoned image. However, most of these triggers are perceptually obvious and are easy to be detected or removed. To improve the stealthiness of backdoor attacks, some dynamic invisible trigger generation methods have been proposed, including sample-specific invisible triggers generated by the DNN-based image steganography [29], [41] or autoencoder neural network [34], random noise optimizations by adversarial perturbation [40], [47], [59], image warping [9], [33], etc. Most backdoor attacks mentioned above mainly focus on adding perturbation in the spatial domain. However, Wang et al. [46] indicated that small perturbations in the frequency domain could produce perturbations dispersed across the entire image, and they proposed a backdoor attack called FTROJAN which injects triggers in mid- and/or high-frequency components of UV channel by Discrete Cosine Transform (DCT). Besides, Feng et al. [14] embed a trigger into the amplitude spectrum while maintaining the phase spectrum unchanged by utilizing Discrete Fourier Transform (DFT) [5].

Different from DFT and DCT, the wavelet transform has spatial directionality and can etract the detailed information such as edges, contours and textures of the image. In addition, the wavelet transform has the ability of multi-resolution

analysis. Drager et al. [13] propose a wavelet transformbased attack (WABA) method which injects the trigger image into the lowest-frequency components of poisoned images by wavelet transform. However, in most cases, it is difficult to maintain the naturalness of the poisoned images by injecting trigger information into the low-frequency region. Wavelet packet decomposition (WPD) is an improvement based on the wavelet transform, which is able to subdivide both high and low frequency information, while wavelet transform can only subdivide low frequency information. Analysing the dataset by WPD to infer the key frequency regions that the DNNs focus on is conducive to the proposal of an effective and precise backdoor attack method. In addition, how to design the trigger information to ensure the effectiveness of the backdoor attack while also making the poisoned images stealthy needs to be further explored.

B. Backdoor Defense

Backdoor defense can be broadly divided into three categories, which are pre-training, in-training, and post-training. For pre-training methods, the defender aims to detect poisoned samples in the training dataset by capturing the anomalous behavior characteristics of poisoned samples, such as activation of samples (e.g. AC [6], Beatrix [31], SCAn [42], Spectral [44], and SPECTRE [20]) and the prediction consistency of samples (e.g. CT [36] and ASSET [35]). For in-training methods, defenders distinguish poisoning samples and benign samples by the difference of their training loss [27] or feature gathering [7], [22], [57], and then unlearn these samples or securely retrain a clean model on the processed dataset. For post-training methods, the defenders remove the embedded backdoors by snipping out possible backdoor neurons, including ANP [53], CLP [61], and NAD [28], or fine-tuning the backdoored model to mitigate backdoor [48], [63]. Furthermore, defenders are capable of reversing backdoor triggers and then pruning backdoor models using these trigger-stamped samples, such as in the NC [45] method, or by rejecting queries once the inputs are identified as poisoned samples (e.g. STRIP [16], SCALE-UP [19], and TeCo [30]).

III. METHOD

A. Preliminary

Wavelet Packet Decomposition (WPD) can transform an image from the spatial domain to the frequency domain and decompose it into multiple frequency regions containing different semantic information. It inherits the time-frequency analysis characteristics of the wavelet decomposition (WD). The main difference is that WD can only decompose low frequency, while WPD can decompose information in every frequency band. The input image x is transformed to a spectrogram which contains low frequency 'a', high-horizontal frequency 'h', high-vertical frequency 'v', high-diagonal frequency 'd'. Taken an image from CIFAR-10 as an example in the Fig. 1, the image in the level-2 spectrogram contains 16 sub-spectrograms with different semantic information.

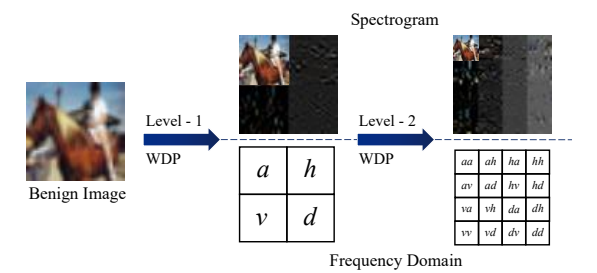


Fig. 1. The principle of wavelet packet decomposition.

B. Problem Formulation

a) Notations: We denote a deep learning based image classifier as $f_{\boldsymbol{\theta}}: \mathcal{X} \to \mathcal{Y}$, where $\boldsymbol{\theta}$ is the model parameter, $\mathcal{X} \in \mathbb{R}^3, \mathcal{Y} = \{1, 2, \dots, c\}$ indicate the input and output space, respectively. The benign training dataset is denoted as $\mathcal{D} = \{(\boldsymbol{x}^{(i)}, y^{(i)})\}_{i=1}^n$, where $\boldsymbol{x}^{(i)} \in \mathcal{X}$ denotes a benign image, while $y^{(i)}$ is its ground-truth label. It will be splitted to two parts, including \mathcal{D}_c and \mathcal{D}_p , and the images in \mathcal{D}_p are selected to generate poisoned images, *i.e.*, $(\boldsymbol{x}^{(i)}, y^{(i)})$ is modified to $(\boldsymbol{x}^{(i)}_{\xi}, t)$ by injecting a trigger $\boldsymbol{\xi}$ into $\boldsymbol{x}^{(i)}$ and changing $y^{(i)}$ to the target label t. The set of poisoned image pairs is denoted as $\hat{\mathcal{D}}_p = \{(\boldsymbol{x}^{(i)}_{\xi}, t) | (\boldsymbol{x}^{(i)}, y^{(i)}) \in \mathcal{D}_p\}$). Then, the poisoned training dataset is $\hat{\mathcal{D}} = \{\mathcal{D}_c, \hat{\mathcal{D}}_p\}$, and the poisoning ratio is $p = \frac{|\hat{\mathcal{D}}_p|}{|\hat{\mathcal{D}}_p|}$.

b) Threat Model: In this work, we consider the data poisoning-based backdoor attack, where the attacker can only manipulate the benign training dataset \mathcal{D} to obtain the poisoned training dataset $\hat{\mathcal{D}}$, without access to the training process. At the inference stage, given the model f_{θ} trained on $\hat{\mathcal{D}}$ by the user, the attacker can generate the poisoned image by injecting the trigger pattern into the benign inference image, and aims to activate the backdoor in the model f_{θ} , *i.e.*, $f_{\theta}(x_{\xi}) = t$.





(a) Image

(b) Image without low frequency

(c) Image without high frequency

Fig. 2. The influence of high and low frequency information on image vision.

C. Analysis on Dataset

In order to make the attack methods more stealthy and precise, we analyze the datasets to infer the key frequency regions in the spectrograms that DNNs would focus on. The key frequency regions would be selected as the poisoning regions. We utilize the N-level WPD to decompose the frequency information of training samples in the datasets and 4^N sub-spectrograms in 4^{N-1} parent-spectrograms can be obtain, i.e., each parent-spectrogram includes 4 sub-spectrograms. We calculate the effectiveness E of the frequency information in each sub-spectrogram for all training samples in the dataset \mathcal{D} ,

which is defined in Eq. (1), *i.e.*, the magnitude of the absolute average of the coefficient in each sub-spectrogram.

$$\begin{cases} C_{s,p}^{N} = \{\sum_{x^{(i)} \in \mathcal{D}} \mathcal{W}^{N}(x^{(i)})\}_{s,p}, \\ E_{s,p}^{N} = \left| \operatorname{avg}(C_{s,p}^{N}) \right|, \end{cases}$$

$$(1)$$

where $C_{s,p}^N$ represents the coefficient matrix of s-th subspectrogram in p-th parent-spectrogram, and $s \in [1,4]$, $p \in [1,4^{N-1}]$. \mathcal{W} represents WPD, which converts the image from the spatial domain to the spectrogram, N is the level of WPD. A larger E indicates the dataset has a higher presence of components within the corresponding sub-spectrogram, and we refer such sub-spectrogram as the key frequency regions. We erase the low frequency and high frequency information of an image respectively, and Fig. 2 shows that the lowest frequency information always plays an impact on image in visual. It is difficult to maintain the visual naturalness after modifying the lowest frequency. Therefore, we do not take into account the information of the lowest frequency when we conduct statistical analysis.

Algorithm 1 Key Regions Selection

```
Input: The benign training dataset as \mathcal{D} = \{x^{(1)}, \dots, x^{(n)}\}\,
        the level of WPD N.
  1: p_{list} = \lceil \rceil
 2: for p = 1, \dots, 4^{N-1} do
             s_{list} = []
            \begin{aligned} & \textbf{for } s \leftarrow 1 \textbf{ to 4 do} \\ & C_{s,p}^N = \{\sum_{x^{(i)} \in \mathcal{D}} \mathcal{W}^N(x^{(i)})\}_{s,p} \\ & E_{s,p}^N = \left|\operatorname{avg}(C_{s,p}^N)\right| \\ & s_{list}.\operatorname{append}(E_{s,p}^N) \end{aligned}
  6:
  7:
             end for
  8:
  9:
             if p=1 then
                  s_{list} = s_{list}.remove(max(s_{list}))
 10:
                 p, s^* = \underset{p, s}{\operatorname{arg\,max}} \{s_{list}\}
 11:
 12:
                  p, s^* = \operatorname*{arg\,max}_{p,s} \{s_{list}\}
 13:
 14:
             p_{list}.append(\{p, s^*\})
 15:
 16: end for
 17: return p_{list}
```

The complexity of the dataset is affected by the number of categories, image volume, etc. The datasets with more categories or larger image volume tend to be more complex and are required to be analysed with more detailed decomposition, i.e., a higher level WPD. We regard the sub-spectrograms in each parent-spectrogram with most effective information as the key frequency regions. Take CIFAR-10 as an example, Fig. 3 illustrates the frequency information distribution of CIFAR-10 decomposed by 2-level WPD, and the parent-spectrograms are the frequency regions in the 1-level WPD, i.e., 'a', 'h', 'v', 'd'. The lowest frequency 'aa' is not counted in the statistics. As a result, the sub-spectrograms of 'ah', 'ha', 'va', 'dh' in each parent-spectrograms contain the most effective information.

The details are shown in Algorithm 1.

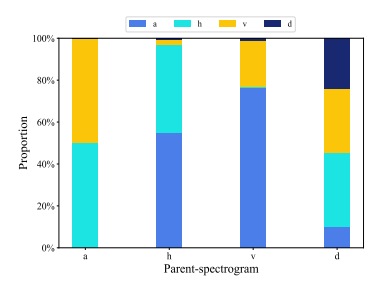


Fig. 3. Frequency information distribution of CIFAR-10 in the spectrogram. (The x-axis represents the parent-spectrogram, and the y-axis represents the percentage of each sub-spectrogram in the parent-spectrogram).

D. Proposed Method

Here we elaborate the proposed WPD-based backdoor attack, dubbed WPDA. Since we focus on data poisoning-based attack, we only describe how to generate the poisoned dataset and inject backdoor, including three main steps in Fig. 4:

1) Generating the poisoned training samples. Selecting 4^{N-1} key frequency regions as the poisoning frequency regions according to Algorithm 1 and generating the poisoned training samples \hat{x}_{train} by Eq. (2):

$$g(x_{train}; k) = \mathcal{W}^{-N}(\mathcal{W}^{N}(x_{train}) \odot m + k \cdot (\mathcal{T}(\mathcal{W}^{N}(\xi)))$$
$$\odot (1 - m))),$$

where $\hat{x}_{train} = g(x_{train}; k)$, ξ represents the trigger image, $m \in \{0,1\}^{2^N \times 2^N \times 3}$ is a binary mask, k is the trigger intensity of the poisoned training samples \hat{x}_{train} . We perform a transformation \mathcal{T} of the trigger in the spectrogram, i.e., each element value is replaced by the average value of the coefficient in sub-spectrogram. The transformation \mathcal{T} not only simplifies the trigger information but also improves the stealthiness of the trigger in visual. In the poisoned training samples, we mask information of the original image in the poisoning frequency regions to promote the model to effectively capture and learn the trigger information.

2) Backdoor injection. Backdoor are injected into the model when the user trains the model by the poisoned training dataset $\hat{\mathcal{D}}_p$. The loss function for model training is shown in Eq. (3):

$$\min_{\theta} \mathcal{L}((f_{\theta}(\hat{\boldsymbol{x}}_{train}), t) + (f_{\theta}(\boldsymbol{x}_{train}), y)). \tag{3}$$

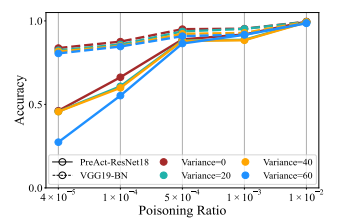
3) Generating the poisoned testing samples. In practical application scenarios, we need to consider the visual performance of the poisoned testing samples, so we retain the information of the original image with the intensity of α in the poisoning frequency regions at the stage of generating the poisoned testing samples \hat{x}_{test} . The poisoned testing samples are generated as Eq. (4):

$$g'(x_{test}; k') = \mathcal{W}^{-N}((k' \cdot (\mathcal{T}(\mathcal{W}^{N}(\xi))) + \alpha \cdot \mathcal{W}^{N}(x_{test}))$$
$$\odot (1 - m) + \mathcal{W}^{N}(x_{test}) \odot m),$$

where $\hat{x}_{test} = g(x_{test}; k')$, k' is the trigger intensity and α is the original information intensity of the poisoned testing samples \hat{x}_{test} .

E. Qualitative Analyses

Take CIFAR-10 as an example and we choose "Hello Kitty" image as the source to generate trigger information. The improvement of the trigger is approached from three perspectives: simplicity, prominence and stealth. *Simplicity* describes the simplicity of the frequency domain information of the trigger; *Prominence* describes the prominence of the trigger message to the model; *Stealthiness* describes the visual invisibility of triggers in the poisoned samples. We generate a validation dataset using the same model as the poisoned training dataset and analyse the impact of triggers with different characteristics on the model based on the accuracy of the model on the validation dataset.



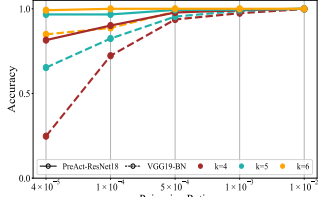


Fig. 5. Simplicity of trigger.

Fig. 6. Prominence of trigger.

- a) Simplicity: We change the simplicity of the trigger information by adding Gaussian noise to the trigger, and Gaussian noise with large varience will decrease the simplicity of the trigger among the poisoned samples. We train the model using training samples with Gaussian noise and then test the performance of the model using validation samples with Gaussian noise. Fig. 5 illustrates that complex triggers increase the difficulty for models to learn triggers. The models with high poisoning ratios are better at learning triggers than the model with low poisoning ratios, which means simple trigger information is more conducive to the effective attack of models with low poisoning ratios.
- b) **Prominence**: In order to guide the model to focus on the trigger information, we erase the original information in the poisoning frequency regions and then add the trigger with different intensty k. We control the prominence of trigger information by modifying the k value, then analyze the effects of triggers with different k value on the model according to accuracy of the poisoned validation dataset. Fig. 6 illustrates that high-intensity trigger information can improve the effectiveness of the attack on both PreAct-ResNet18 and VGG19-BN, especially at extremely low poisoning ratios.
- c) Stealthiness: We suppose that the original information has the negative effect on the backdoor activation, but the model has a limited generalization ability. After assuring that the model is able to learn the trigger information effectively (i.e., the triggers are prominent enough and the trigger information is simple enough during the training stage), we retain the frequency information of the original image with the intensity α to the poisoned validation samples and analyze the

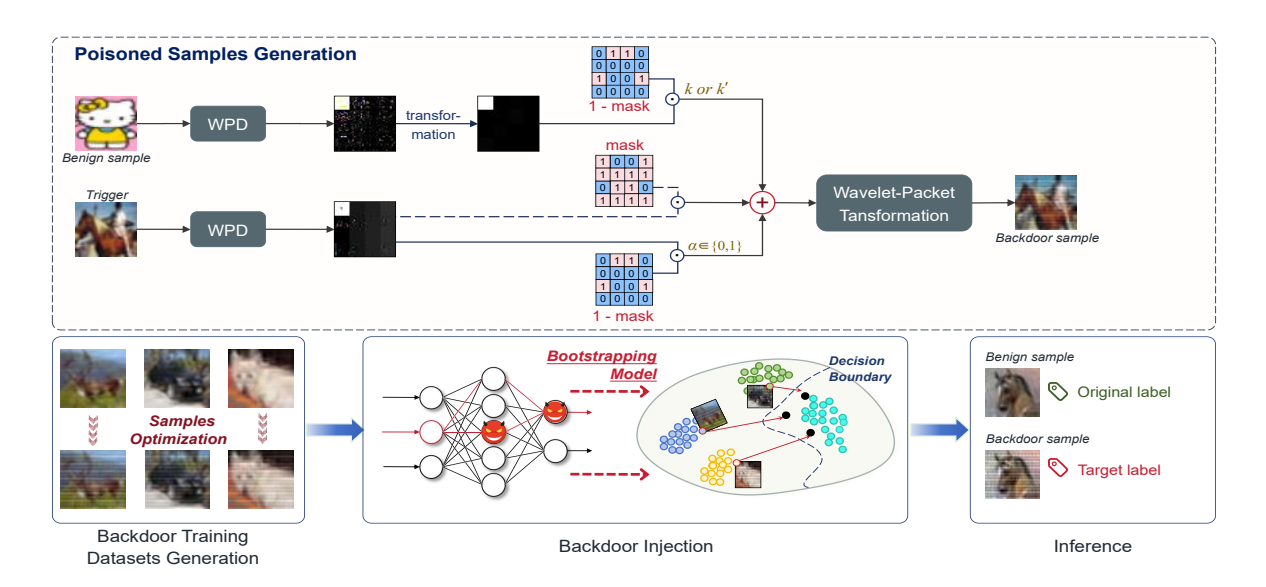
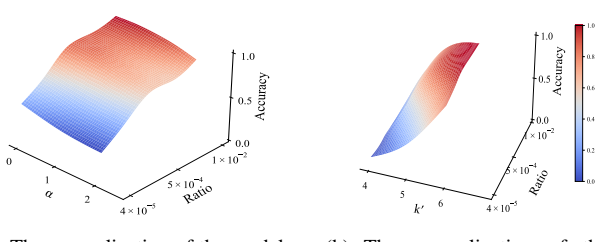


Fig. 4. Overview of WPDA. The process of data-poisoning backdoor attacks includes three stages. In stage one, attackers design and inject the trigger into the benign samples. In stage two, the poisoned training samples will bootstrap the model to change decision boundaries during model training process. In stage three, the model trained by poisoned training samples can classify the poisoned testing samples into the target class and the benign testing samples into the original class. *Poisoned Samples Generation* module describes the process of poisoned samples generation, including the poisoned training and the poisoned testing samples.



(a) The generalization of the model on the original image information

(b) The generalization of the model on the trigger information

Fig. 7. Taking CIFAR-10 trained on VGG19-BN as an example. In the **left**, we set k=6 and analyze the effect of the intensity of the original image information α on the generalization of the model. In **right**, we set $\alpha=1$ and analyze the effect of the intensity of the trigger information k' on the generalization of the model.

generalization of the models under different poisoning ratios according to the accuracy of the poisoned validation dataset. There are obvious differences in the generalization of models with different poisoning ratios in Fig. 7(a). When α increases, the accuracy of the poisoned validation dataset gradually decreases. While, the backdoor models trained by the datasets with high concentration of poisoned samples have strong generalization ability. Similarly, we set $\alpha = 1$ and modify the trigger intensity k' in the poisoned validation dataset. As shown in Fig. 7(b), poisoned validation samples with intense triggers promote the model to capture the information of the triggers. Besides, we also find out that the backdoor models trained by datasets with high concentration of poisoned training samples still have strong generalization ability, which means that their performance reaches over-saturation. Therefore, we are supposed to retain the original information with intensity α and set different trigger information intensity k' of the trigger in the poisoned testing samples at different the poisoning ratios.

IV. EXPERIMENTS

A. Experiment Settings

- a) Datasets and Models: We conduct experiments on three benchmark datasets, including CIFAR-10 [23], CIFAR-100 [23] and Tiny ImageNet [25]. Specifically, CIFAR-10 [23] contains 10 classes with 60,000 color images and the size of each image is $32 \times 32 \times 3$. There are 50,000 images for training and 10,000 images for testing. CIFAR-100 [23] has 100 classes, each of them containing 500 training images and 100 testing images. The size of an image in CIFAR-100 is the same as that in CIFAR-10 [23]. Tiny ImageNet [25] is a subset of ImageNet [11] which contains 200 classes, with 500 images per class for training, 50 images per class for validation, and 50 images per class for testing. The size of each image is $64 \times 64 \times 3$. The model architectures that we adopted are PreAct-ResNet18 [21] and VGG19-BN [39].
- b) Attack Settings: We compare the proposed method with seven current state-of-the-art (SOTA) backdoor attacks, which can be divided into four categories: 1) non clean-label with spatial-statistic trigger, such as BadNets [18] and Blended [8]; 2) non clean-label with spatial-dynamic trigger, like SSBA [29] and Input-Aware [32]; 3) clean-label with spatial-statistic trigger, like SIG [4]; 4) non clean-label with frequency-statistic trigger, including LF [58] and WABA [13]. To verify the effectiveness of our method, we compare the attack performance with the SOTA attacks under different poisoning ratios, ranging from 0.004% to 1%. It is worth noting that 0.004% means that there are only 2 poisoned samples in the training dataset of CIFAR-10 [23] and CIFAR-100 [23], and 4 poisoned samples in the training dataset of Tiny ImageNet [25].
- c) Defense Settings: We validate the performance of our method against multiple popular backdoor defense and detection methods. There are three backdoor detection methods

(e.g. AC [6], SCAn [42], and STRIP [16].) and five SOTA backdoor defense methods (e.g. CLP [61], FT, I-BAU [57], NAD [28], and NC [45].) are considered. For the detection methods, SCAn [42] and STRIP [16], which assume that a detector can access a small set of benign samples, we assume the number of benign samples for each class to be 10, as recommended in these works. For the defense methods, we follow the default configuration used in BackdoorBench [51], [52] for a fair comparison.

		CIFAR-100								Tiny ImageNet											
aa	ah	ha	hh	hh -	aaa	aah	aha	ahh	haa	hah	hha	hhh		aaa	aah	aha	ahh	haa	hah	hha	hhh
uu	un	m	1111		aav	aad	ahv	ahd	hav	had	hhv	hhd		aav	aad	ahv	ahd	hav	had	hhv	hhd
av	ad	hv	hd		ava	avh	ada	adh	hva	hvh	hda	hdh		ava	avh	ada	adh	hva	hvh	hda	hdh
av	au	11 V	IIU		avv	avd	adv	add	hvv	hvd	hdv	hdd		avv	avd	adv	add	hvv	hvd	hdv	hdd
va	vh	da	dh		vaa	vah	vha	vhh	daa	dah	dha	dhh		vaa	vah	vha	vhh	daa	dah	dha	dhh
va	VII	ua	un		vav	vad	vhv	vhd	dav	dad	dhv	dhd		vav	vad	vhv	vhd	dav	dad	dhv	dhd
	1	4	dd		vva	vvh	vda	vdh	dva	dvh	dda	ddh		vva	vvh	vda	vdh	dva	dvh	dda	ddh
VV	vd	dv	aa		vvv	vvd	vdv	vdd	dvv	dvd	ddv	ddd		vvv	vvd	vdv	vdd	dvv	dvd	ddv	ddd

Fig. 8. The selected regions for CIFAR-10, CIFAR-100, and Tiny ImageNet, respectively.

- d) Details of WPDA: According to the description of WPDA shown in Sec. III, we will provide more details about the decomposition level of dataset, the selection of the poisoning regions, and the design of the trigger.
 - Dataset Decomposition. Datasets with large volumes and numerous categories are often complex, requiring detailed decompositions to achieve effectiveness at extremely low poisoning ratios. Hence, in the experiment, we perform a 2-level WPD on CIFAR-10, while CIFAR-100 and Tiny ImageNet undergo a 3-level WPD.
 - 2) Poisoning Regions Selection. Based on the analysis in Sec. III-C, 4^{N-1} key poisoning regions of subspectrograms are selected as the poisoning regions (except the lowest frequency region in the spectrogram). We highlight the selected regions in Fig. 8, in which it can be seen that there are four regions chosen in CIFAR-10 and 16 regions in CIFAR-100 and Tiny ImageNet.
 - 3) Trigger Design. In the following experiment, we select "Hello Kitty" image as the trigger. For different datasets, the trigger information intensity k in the poisoned training samples is altering, such as k=6 in CIFAR-10, k=8 in CIFAR-100, and k=7 in Tiny ImageNet. The values of the trigger information intensity k' in the poisoned testing samples for different datasets can be referred to Tab. I, and the original information intensity α is 1.
- e) Evaluation Metrics: To evaluate the attack performance of our proposed method, we adopt two metrics: Clean Accuracy (C-Acc), defined as the prediction accuracy on all benign testing samples by the trained model, and Attack Success Rate (ASR), which measures the accuracy of poisoned testing samples being correctly predicted as the target class. The higher C-Acc and higher ASR imply better attack performance. Furthermore, to assess the performance of detection methods, we utilize three metrics: True Positive Rate (TPR), False Positive Rate (FPR), and Weighted F1 Score $(F_1^\omega = \frac{2TP}{2TP+FP+\omega FN'})$ used in [55]. TPR reflects the accuracy with which detection methods identify poisoned

samples, while FPR indicates the rate at which benign samples are mistakenly classified as poisoned. F_1^{ω} is one variant of F_1 score, which quantifies the detection method's ability to accurately classify poisoned samples while minimizing the misclassification of benign samples.

TABLE I THE VALUE OF k^\prime IN Eq. (4) under the condition of different poisoning ratios on datasets.

Poisoning ratio → Dataset ↓	0.004%	0.01%	0.05%	0.1%	1%
CIFAR-10	8	8	6	6	6
CIFAR-100	10	8	7	6	5
Tiny ImageNet	8	8	7	7	7

B. Attack Performance of WPDA

- a) Evaluations on CIFAR-10: Tab. II illustrates the attack performance of the compared attack methods and our method on CIFAR-10 with various poisoning ratios. It is evident that other attacks cannot achieve good attack performance under the extremely low poisoning ratio of 0.004%. In this situation, the highest ASR achieved by Input-Aware is 12.36% on Preact-ResNet18 and 10.19% on VGG19-BN, respectively. In contrast, WPDA can achieve ASRs of 98.12% on Preact-ResNet18 and 77.50% on VGG19-BN. As the poisoning ratio increases, there is a significant improvement in attack performance. WPDA can achieve ASRs of 100% on Preact-ResNet18 and 99.99% on VGG19-BN. From Tab. II, it is also evident that one advantage of low poisoning ratio attacks is their minimal impact on clean accuracy. Moreover, the C-Acc of WPDA is the highest among the compared attacks at a poisoning ratio of 0.004\%, reaching 94.03\% on Preact-ResNet18 and 92.49% on VGG19-BN, respectively.
- b) Evaluations on CIFAR-100: From Tab. III, we notice that the highest ASR achieved by the compared methods is 1.29% on Preact-ResNet and 1.04% on VGG19-BN, which underscores the challenge of successfully embedding a backdoor at a poisoning ratio of 0.004%. At the same poisoning ratio, the ASR of WPDA can reach 85.01% on Preact-ResNet and 79.94% on VGG19-BN, respectively. It can be seen that WPDA consistently outperforms other attacks at the previous four poisoning ratios, but is surpassed by WABA at 1% poisoning ratio. However, poisoned samples generated by WPDA are more natural and less visible to the naked eyes than those generated by WABA.
- c) Evaluations on Tiny ImageNet: The attack performance on Tiny ImageNet is shown in Tab. IV. Similar to CIFAR-100, the compared methods cannot achieve a high ASR on Tiny ImageNet at a 0.004% poisoning ratio. However, WPDA can still achieve an 80.99% ASR on PreAct-ResNet18 and 64.96% ASR on VGG19-BN with only 4 poisoned samples, both far exceeding the values achieved by the compared methods. If the compared methods aim to achieve the same level of attack performance, they would need to poison a larger number of samples, such as 1,000 samples in the training dataset of Tiny ImageNet. Due to the limited number of samples in each class, we are unable to conduct SIG on this

TABLE II
THE RESULT OF 7 COMPARED ATTACK METHODS AND OUR METHOD UNDER 5 DIFFERENT POISONING RATIOS IN THE CIFAR-10

	Poisoning ratio \rightarrow	0.00	14%	0.0	1%	0.0	5%	0.1	%	11	%
	Attack ↓	C-Acc	ASR								
	BadNets [18]	93.68	0.67	93.74	0.88	93.70	26.07	93.61	1.23	93.14	74.73
PreAct-ResNet18	Blended [8]	94.21	4.81	94.00	7.49	93.81	26.07	93.80	56.11	93.76	94.88
Š	Input-aware [32]	91.54	12.36	90.28	13.73	90.66	38.78	91.94	47.32	91.74	79.18
Şe	LF [58]	93.93	0.94	93.98	1.22	94.06	1.39	93.55	12.72	93.56	86.46
7,	SIG [4]	93.94	0.53	93.75	1.07	93.93	18.76	94.05	54.88	93.68	87.71
Ä	SSBA [29]	93.81	0.71	94.10	0.59	93.90	1.27	93.89	1.62	93.43	73.44
Pre	WABA [13]	93.95	5.87	93.76	10.62	93.67	68.09	93.77	86.16	93.65	99.19
	WPDA(Ours)	94.03	98.12	93.89	98.71	93.58	99.80	93.84	99.76	93.86	100.00
	BadNets [18]	92.23	0.89	91.96	0.82	92.23	0.94	92.03	1.09	91.73	74.66
-	Blended [8]	92.25	3.41	91.73	5.67	92.32	22.24	92.16	44.10	92.06	92.87
VGG19-BN	Input-aware [32]	89.47	10.19	89.40	11.89	89.62	59.82	89.36	77.16	89.02	67.30
61	LF [58]	92.12	2.30	92.43	0.76	91.94	0.97	92.21	0.92	91.41	1.89
g	SIG [4]	92.14	0.73	91.97	2.31	92.20	12.47	91.96	33.74	92.03	91.06
Š	SSBA [29]	92.26	0.98	92.33	0.97	92.38	1.21	92.36	1.44	91.94	38.39
	WABA [13]	92.08	3.03	92.02	20.74	91.91	48.09	91.87	79.13	92.27	97.93
	WPDA(Ours)	92.49	77.50	92.29	91.79	92.33	99.23	92.50	99.64	92.01	99.99

TABLE III
The result of 7 compared attack methods and our method under 5 different poisoning ratios in the CIFAR-100.

	Poisoning ratio \rightarrow	0.00	14%	0.0	1%	0.0	5%	0.1	%	19	%
	Attack ↓	C-Acc	ASR								
	BadNets [18]	70.83	0.13	70.23	0.17	70.48	0.15	70.80	0.20	70.25	41.51
PreAct-ResNet18	Blended [8]	70.67	0.09	70.60	0.34	70.74	23.37	70.75	52.74	70.48	90.67
Š	Input-aware [32]	65.27	1.11	64.88	5.47	62.93	39.86	64.18	73.11	64.82	73.72
ş	LF [58]	70.72	0.10	70.42	0.09	71.02	0.15	70.85	0.84	70.36	45.55
7	SIG [4]	70.33	0.13	70.38	0.52	70.75	5.04	70.79	11.19	69.81	77.85
ŞΑ	SSBA [29]	70.32	0.05	70.48	0.11	70.64	0.15	70.31	0.40	70.18	44.05
Pre	WABA [13]	70.18	1.29	70.37	24.46	70.44	71.23	70.28	86.48	70.42	98.56
	WPDA(Ours)	70.28	85.01	70.56	89.01	70.71	95.32	70.44	93.22	70.32	95.74
	BadNets [18]	66.06	0.15	65.68	0.20	65.64	0.23	65.62	0.32	65.53	69.31
_	Blended [8]	65.34	0.07	65.25	0.08	65.31	14.62	65.65	37.05	65.57	88.12
BN	Input-aware [32]	58.01	1.04	57.94	1.46	60.37	1.00	59.87	38.35	59.78	36.63
VGG19-BN	LF [58]	65.47	0.17	66.11	0.08	65.59	0.25	65.61	0.27	65.30	0.69
g	SIG [4]	65.45	0.31	65.49	0.09	65.89	4.60	65.34	14.73	65.13	72.02
Š	SSBA [29]	65.56	0.09	65.84	0.08	66.14	0.28	65.84	0.52	64.87	13.03
	WABA [13]	65.40	0.40	65.57	7.61	65.48	65.72	66.20	85.47	65.59	97.64
	WPDA(Ours)	66.24	79.94	65.18	88.09	65.62	97.20	65.47	91.06	65.13	94.58

dataset, which is a clean-label attack and only injects the trigger to the target class.



Fig. 9. Visualization of the poisoned samples in datasets.

d) In summary: The above comparisons demonstrate the superior attack performance of WPDA compared to 7 SOTA attacks, especially at low poisoning ratios. Fig. 9 shows the visualization of the poisoned samples on CIFAR-10, CIFAR-100 and Tiny ImageNet. Compared with other attack methods, Although the backdoor samples based on WPDA method is not the most natural to the original image in visual, WPDA balances the effectiveness of the backdoor attack and the naturalness of the samples at a very low poisoning ratio.

C. Detection Performance of WPDA

To evaluate the performance of WPDA against current detection methods, we applied three detectors to WPDA across

three datasets and two models, using five different poisoning ratios. The results are shown in Tab. V and Tab. VI.

- a) Evaluations on AC: From Tab. V and Tab. VI, we notice that AC fails to correctly identify poisoned samples in the training datasets when the poisoning ratio is less than 1% across both model structures. Indeed, AC has misclassified many benign samples as poisoned; for instance, it exhibits a 11.31% FPR in CIFAR-10 at a 0.05% poisoning ratio. We conjecture that this is because the number of poisoned samples is too small to be recognized as a distinct cluster by AC. Meanwhile, the activations of some benign samples are incorrectly divided into two clusters, with the smaller one being misidentified as poisoned. When the poisoning ratio is 1%, AC can achieve 99.40% TPR and 7.31% FPR on CIFAR-10 trained by VGG19-BN.
- b) Evaluations on SCAn: SCAn, another detection method based on activations, is found to be ineffective at all poisoning ratios on PreAct-ResNet18. However, when applied to VGG19-BN, SCAn successfully detects poisoned samples, achieving a 98.40% TPR on CIFAR-10 and 99.10% TPR on Tiny ImageNet at a 1% poisoning ratio. Yet, it fails to identify poisoned samples at the previous four poisoning ratios with VGG19-BN. These observations illustrate that: 1) at extremely low poisoning ratios, the EM algorithm utilized by SCAn fails to recognize the target class as a mixed distribution; 2) the effectiveness of this detection method depends on the

TABLE IV The result of 7 compared attack methods and our method under 5 different poisoning ratios in the Tiny ImageNet.

	Poisoning ratio \rightarrow	0.00	0.004%		1%	0.0	5%	0.1	1%	11	%
	Attack ↓	C-Acc	ASR	C-Acc	ASR	C-Acc	ASR	C-Acc	ASR	C-Acc	ASR
	BadNets [18]	56.87	0.12	56.86	0.18	57.26	0.25	57.51	33.53	57.51	95.01
~=	Blended [8]	57.24	0.06	57.11	2.90	57.68	50.88	57.58	65.19	57.31	95.29
PreAct-ResNet18	Input-aware [32]	58.55	2.00	57.93	34.96	58.05	57.29	57.96	63.80	57.94	85.12
es	LF [58]	56.98	0.17	57.03	0.13	57.26	0.16	56.97	19.49	56.47	83.03
7.	SIG [4]	57.11	4.14	57.16	10.32	56.86	27.42	57.03	44.93	_	_
Ϋ́	SSBA [29]	56.80	0.11	56.96	0.30	57.23	2.31	57.20	13.28	56.88	80.43
Pre	WABA [13]	57.10	4.13	57.30	15.92	56.51	74.14	57.17	90.13	56.82	98.37
	WPDA(Ours)	57.24	80.99	56.88	85.80	56.73	88.45	56.86	90.71	57.28	98.53
	BadNets [18]	53.65	0.24	53.99	0.18	53.87	0.38	54.85	48.85	53.48	98.86
_	Blended [8]	53.77	0.23	53.71	5.88	53.53	52.88	53.43	69.38	52.47	94.90
BN	Input-aware [32]	53.80	8.91	53.98	17.71	53.92	35.13	54.09	85.43	54.10	79.82
VGG19-BN	LF [58]	54.02	0.16	53.28	0.17	53.25	0.22	52.80	0.22	51.94	0.51
Ö	SIG [4]	53.35	3.09	54.24	1.65	53.62	12.41	53.33	26.92	_	_
\geq	SSBA [29]	54.15	0.02	53.17	0.22	54.35	2.42	53.91	8.42	53.10	86.63
	WABA [13]	52.43	9.76	53.20	24.90	53.80	80.37	53.80	93.40	53.22	98.50
	WPDA(Ours)	53.46	64.96	54.25	81.89	53.74	91.96	53.99	90.30	51.39	96.03

TABLE V
THE RESULT OF WPDA AGAINST 3 DETECTION METHODS UNDER 5 DIFFERENT POISONING RATIOS IN THE DATASETS. THE TRAINING MODEL ADOPTS
PREACT-RESNET18.

Dataset	Poisoning ratio \rightarrow	(0.004%		0.01%				0.05%			0.1%		1%		
	Detection \downarrow	TPR	FPR	F_1^{ω}	TPR	FPR	F_1^{ω}	TPR	FPR	F_1^{ω}	TPR	FPR	F_1^{ω}	TPR	FPR	F_1^{ω}
	AC [6]	0.00	0.00	0.00	0.00	0.00	0.00	0.00	0.00	0.00	0.00	0.00	0.00	0.00	0.00	0.00
CIFAR10	SCAn [42]	0.00	0.00	0.00	0.00	0.00	0.00	0.00	0.00	0.00	0.00	0.00	0.00	0.00	0.00	0.00
CIFAKIU	STRIP [16]	50.00	8.00	0.05	20.00	8.15	0.05	44.00	8.29	0.51	56.00	10.29	1.04	93.80	12.25	12.88
	AC [6]	0.00	0.97	0.00	0.00	0.28	0.00	0.00	0.48	0.00	0.00	0.92	0.00	0.00	0.93	0.00
CIFAR-100	SCAn [42]	0.00	0.00	0.00	0.00	0.00	0.00	0.00	0.00	0.00	0.00	0.00	0.00	0.00	0.00	0.00
CIFAK-100	STRIP [16]	0.00	14.66	0.00	0.00	12.56	0.00	48.00	13.06	0.36	76.00	12.47	1.19	100.00	8.31	19.56
	AC [6]	0.00	1.07	0.00	0.00	0.68	0.00	0.00	0.58	0.00	0.00	0.67	0.00	0.00	1.60	0.00
Tiny ImagaNat	SCAn [42]	0.00	0.00	0.00	0.00	0.00	0.00	0.00	0.00	0.00	0.00	0.00	0.00	99.90	0.00	99.50
Tiny ImageNet	STRIP [16]	25.00	15.67	0.01	40.00	13.03	0.06	62.00	16.16	0.38	78.00	15.91	0.96	95.70	18.41	9.32

TABLE VI
THE RESULT OF WPDA AGAINST 3 DETECTION METHODS UNDER 5 DIFFERENT POISONING RATIOS IN THE DATASETS. THE TRAINING MODEL ADOPTS VGG19-BN.

Dataset	Poisoning ratio \rightarrow		0.004%			0.01%			0.05%			0.1%		1%		
	Detection \downarrow	TPR	FPR	F_1^{ω}	TPR	FPR	F_1^{ω}	TPR	FPR	F_1^{ω}	TPR	FPR	F_1^{ω}	TPR	FPR	F_1^{ω}
	AC [6]	0.00	8.42	0.00	0.00	10.92	0.00	0.00	11.31	0.00	0.00	11.31	0.00	99.40	7.41	27.17
CIFAR10	SCAn [42]	0.00	0.00	0.00	0.00	0.00	0.00	0.00	0.00	0.00	0.00	4.58	0.00	98.40	0.00	93.18
CIFARIO	STRIP [16]	0.00	10.02	0.00	0.00	13.79	0.00	32.00	6.64	0.46	42.00	8.99	0.88	94.80	12.70	12.69
	AC [6]	0.00	3.67	0.00	0.00	3.03	0.00	0.00	1.24	0.00	0.00	2.57	0.00	0.00	2.03	0.00
CIFAR 100	SCAn [42]	0.00	0.00	0.00	0.00	0.00	0.00	0.00	0.00	0.00	0.00	0.00	0.00	0.00	0.00	0.00
CIFAR100	STRIP [16]	0.00	13.65	0.00	40.00	11.54	0.07	52.00	19.00	0.27	70.00	16.52	0.83	100.00	15.10	11.80
	AC [6]	0.00	2.98	0.00	0.00	6.26	0.00	0.00	7.13	0.00	0.00	7.98	0.00	0.00	18.47	0.00
Time ImageNet	SCAn [42]	0.00	0.00	0.00	0.00	0.00	0.00	0.00	0.00	0.00	0.00	0.00	0.00	99.10	0.00	96.03
Tiny ImageNet	STRIP [16]	0.00	16.70	0.00	0.00	16.27	0.00	10.00	12.88	0.08	9.00	13.74	0.12	47.20	15.58	4.47

activations extracted by the models.

c) Evaluations on STRIP: STRIP is a detection method based on the perturbation of inputs. The principle behind this detection method is that the predictions on perturbed poisoned samples are more consistent than the predictions on benign samples. From Tab. V and Tab. VI, we note that as the poisoning ratio rises, there is a corresponding elevation in the TPR of STRIP across the three datasets when trained on two models. The occurrence of this phenomenon may be attributed to the fact that as the poisoning ratio increases, the model learns more about the trigger, leading to predictions of the target class even with only a partial appearance of the trigger. Consequently, poisoned samples become more readily detectable by STRIP. This phenomenon indicates that the primary advantage of WPDA lies in its ability to evade detection methods at low poisoning ratios.

d) In summary: Based on the above results, it is evident that attacks with high poisoning ratios are more easily to be detected than those with low poisoning ratios. At low poisoning ratios, a few number of poisoned training samples can make anomalous behaviour relatively undetectable.

D. Defense Performance of WPDA

In the following, we evaluate the attack performance of WPDA and other attacks under 5 SOTA backdoor defense methods.

a) Evaluations on CIFAR-10: Fig. 11 illustrates the performance of 7 SOTA attack methods and WPDA against 5 SOTA defense methods. Compared with other attack methods, WPDA shows stable performance after various defense methods at every poisoning ratio. Besides, backdoor attacks at low poisoning ratios are more stable than those at high poisoning

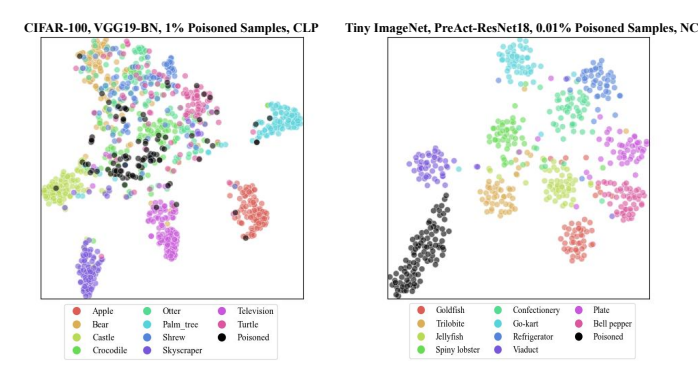


Fig. 10. t-SNE on mixed testing samples after defenses. One color corresponds to one class. We randomly select benign testing samples from 10 classes in the total classes, which also includes benign testing samples in the target class. The black circles represent the poisoned testing samples in target class. (Left: t-SNE on CIFAR-100 after CLP, target class is 'Apple', Right: t-SNE on Tiny ImageNet after NC, target class is 'Goldfish'.)

ratios in some cases. For example, the ASR of attack methods such as Blended, Input-Aware and WPDA at 0.05% poisoning ratio decays less than that at 0.1% poisoning ratios after I-BAU on PreAct-ResNet18, Input-Aware and WABA on VGG19-BN have the same performance after NC.

b) Evaluations on CIFAR-100: Fig. 12 illustrates that WPDA at low poisoning ratios shows advantages after various defense methods. As for PreAct-ResNet18, WPDA achieves optimal performance compared with other attacks at low poisoning ratios. WPDA at low poisoning ratios is even more stable than WPDA at high poisoning ratios, such as against CLP, I-BAU and NC. As for VGG19-BN, results illustrate that attacks at high poisoning ratios increase the risk of failure against defenses, i.e., a significant decay of ASR at high poisoning ratios. Fig. 10(Left) shows the t-SNE on the mixed testing samples of CIFAR-100 after CLP. The poisoned testing samples are clearly separated from benign testing samples in the target class after CLP, which means the model effectively captures the channels related to the backdoor, causing the attack to fail. However, lots of benign samples in other classes overlap in the feature space, which results in a significant drop of the model's accuracy on benign testing samples.

c) Evaluations on Tiny ImageNet: Fig. 13 illustrates WPDA trained by Tiny ImageNet is very stable, not only achieving successful attacks, but remaining effective after the defenses, even at low poisoning ratios. The results also show that the backdoor attacks at low poisoning ratios increase the stealth of the attack, for example, WPDA's ASR decay at low poisoning ratios is less than that at high poisoning ratios against I-BAU on both PreAct-ResNet18 and VGG19-BN. Not only WPDA, Input-Aware trained on PreAct-ResNet18 and VGG19-BN also shows the same performance against NC. What needs to be analysed in particular is the performance of WPDA at 0.01% poisoning ratio after AC. Fig. 10(Right) illustrates that the poisoned testing samples are effectively separated from the samples in the target class. Although the backdoor effect is effectively mitigated by pruning neurons

that are highly correlated with the backdoor, the accuracy of the benign testing samples drops substantially. As for NAD, when the model's attention is shifted, few poisoned training samples cannot promote the model to learn the trigger information effectively, leading to a drop in ASR. Although the effectiveness of WPDA is influenced, the accuracy of the model on benign testing samples decays a lot after NC.

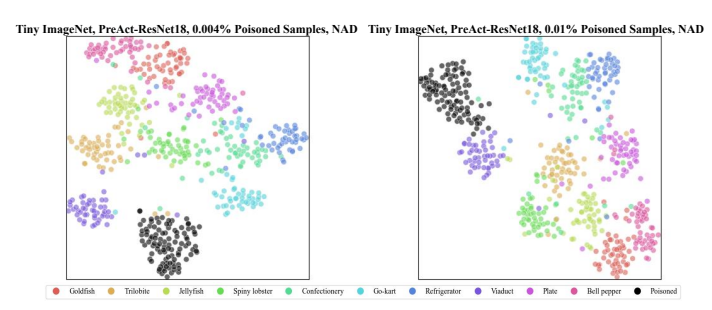


Fig. 14. t-SNE on mixed testing samples of Tiny ImageNet after NAD. NAD remove the backdoor effect of WPDA but the accuracy of benign samples are influenced. (Target Class is 'Goldfish')

d) In summary: Most defense methods are difficult to defend against backdoor attacks with low poisoning ratios, which indicates that it is necessary to explore backdoor attacks at low poisoning ratios. Compared with 7 SOTA attack method, WPDA shows more stable and stealthy performance, especially at low poisoning ratios.

V. ANALYSES

A. Visualization on t-SNE

Fig. 15(b) shows the t-SNE of 7 SOTA attacks and WPDA on PreAct-ResNet18 trained by CIFAR-10 at 1% poisoning ratio. 7 SOTA attacks and WPDA achieve high ASR at 1% poisoning ratio, and the poisoned training samples are close to the benign samples in the target class and the poisoned testing samples, which means that the features extracted by the model from those samples exhibit significant similarity. We conclude that the model effectively learns the trigger rather than memorizing the poisoned training samples. In Fig. 15(a), as for BadNets, Blended, Input-Aware, SIG, SSBA, LF and WABA, the poisoned training samples are close to the benign samples in the target class, while the poisoned testing samples are evenly distributed across the classes. In other words, the models based on these attack methods only memorize the poisoned training samples rather than learning the features of the trigger, which results in the backdoor not being activated when the poisoned testing samples are used as inputs. However, the poisoned training samples generated by WPDA are not only close to the samples in the target class but also to the poisoned testing samples in the feature space, which is consistent with the performance of attacks at 1% poisoning ratio. In summary, WPDA precisely injects trigger information into the key frequency regions, prompting the model to effectively learn the trigger information even at low poisoning ratios.

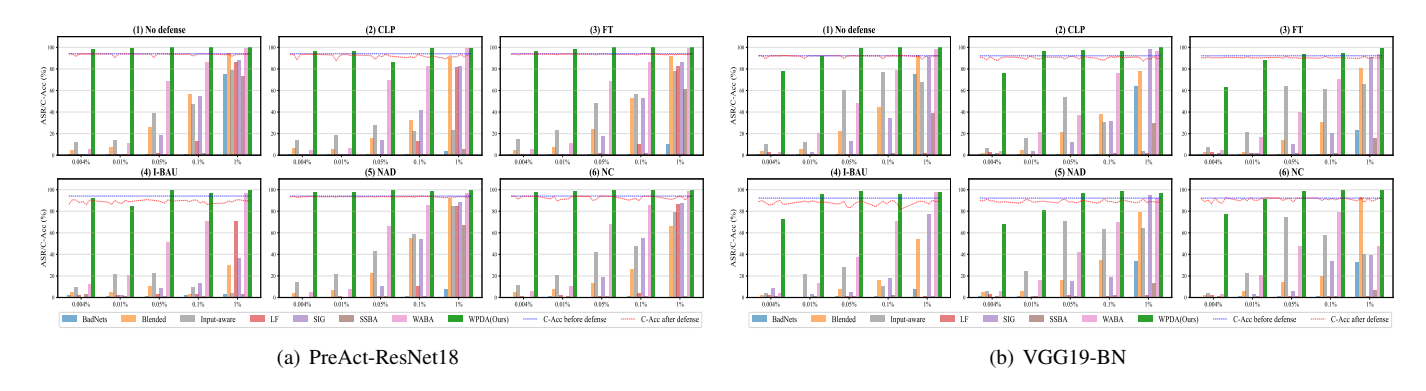


Fig. 11. CIFAR-10 backdoor attack performance under different defenses. Each sub-plot corresponds to one defense method. In each sub-pot, each pillar in the histogram indicates the ASR value of one attack method, and the C-Acc values are represented by dotted curves.

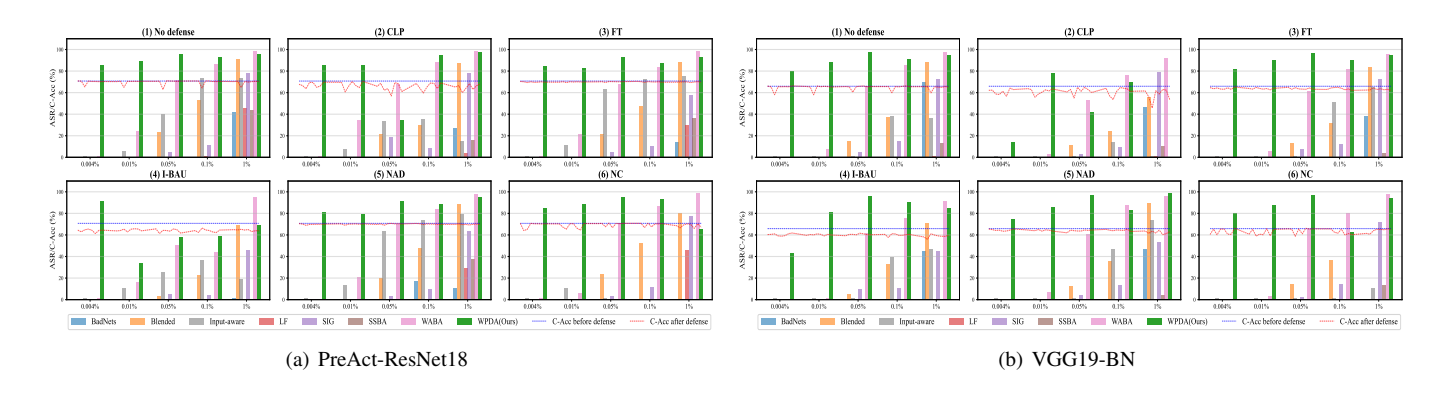


Fig. 12. CIFAR-100 backdoor attack performance under different defenses. Each sub-plot corresponds to one defense method. In each sub-pot, each pillar in the histogram indicates the ASR value of one attack method, and the C-Acc values are represented by dotted curves.

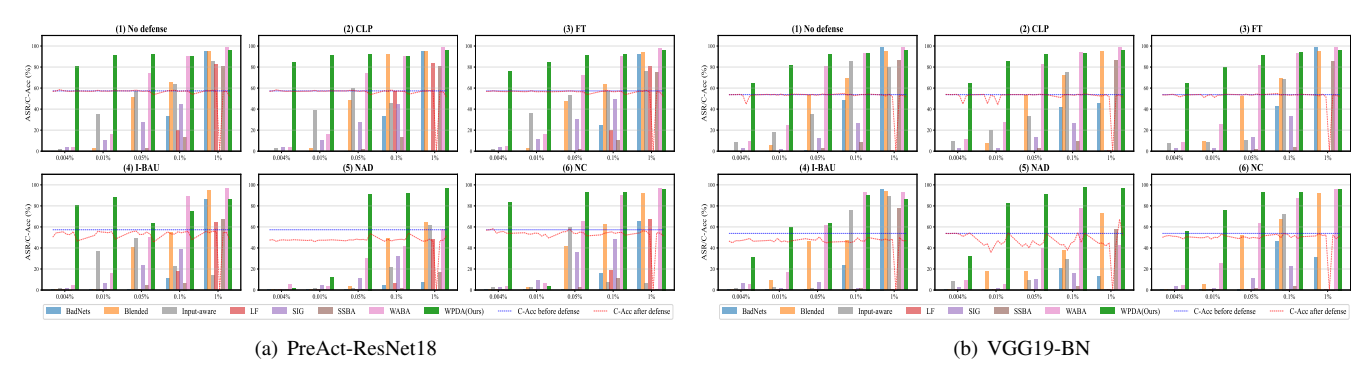


Fig. 13. Tiny ImageNet [25] backdoor attack performance under different defenses on PreAct-ResNet18 [21]. Each sub-plot corresponds to one defense method. In each sub-pot, each pillar in the histogram indicates the ASR value of one attack method, and the C-Acc values are represented by dotted curves.

B. Visualization on l_2 distance KDE

Kernel Density Estimation (KDE) is a non-parametric statistical method for estimating the Probability Density Function (PDF) that can be used to describe the distribution of data [17]. Specifically, KDE is a measure of estimated probability density defined by a kernel function near each data point in the dataset. In KDE, we usually choose a kernel function and a bandwidth parameter to define the similarity between each data point in the dataset and other data points, usually using the Gaussian kernel function, *etc*.

To further verify the effectiveness of the WPDA attack, we conduct l_2 -distance KDE visualization analyses on PreAct-

ResNet18 trained by CIFAR-10 at different poisoning ratios. At first, we extract the features of poisoned samples from the 'linear' layer in PreAct-ResNet18 and calculate the l_2 distance between each poisoned training sample and each poisoned testing sample, then we can obtain multiple lists of l_2 -distance between each poisoned training sample and all poisoned testing samples, where the number of lists is equal to the number of poisoned testing samples and the length of each list is equal to the number of poisoned testing samples. Then average the multiple lists of l_2 -distance and conduct KDE visualization.

In Fig. 16, the horizontal axis represents the average l_2

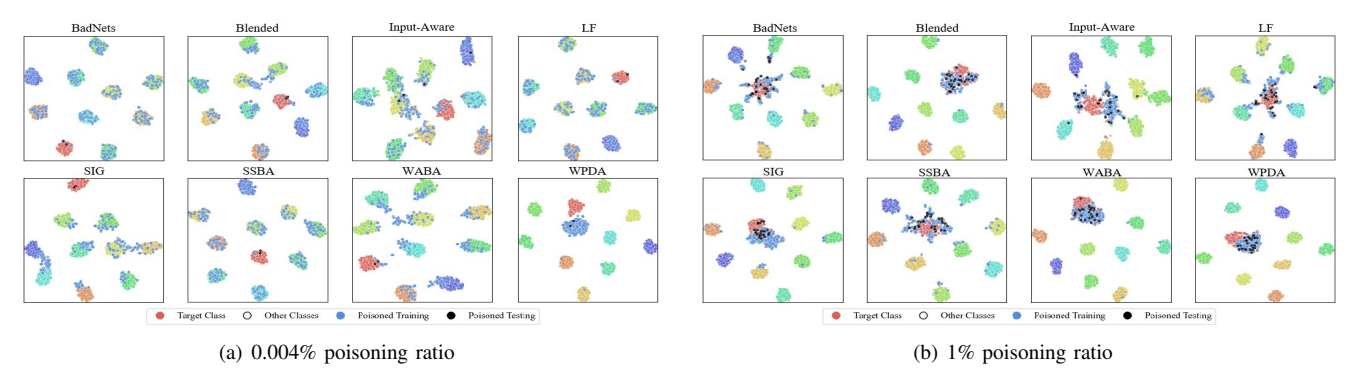


Fig. 15. t-SNE about 7 SOTA attack methods and WPDA at 0.004% and 1% poisoning ratios.

distance between the poisoned training samples and the poisoned testing samples, and the vertical axis represents the density of each l_2 -distance value. The l_2 -distance with a large value means that the features extracted by the model from the poisoned training samples have a large variability from the features extracted from the poisoned testing samples. It is much difficult for the model to predict the poisoned testing samples as target class. At 0.004% poisoning ratio, the l_2 distance in WPDA are mainly concentrated in small values, which indicates that the features extracted by the model from the poisoned testing samples are similar to those extracted in the poisoned training samples. While, for other attacks, the features extracted by the model from the poisoned testing samples differ from those extracted from the poisoned training samples. As the poisoning ratios increases, l_2 -distance value in each attack decreases and concentrates gradually, indicating that the model gradually learns the trigger information.

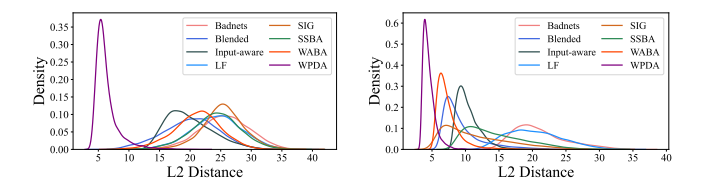
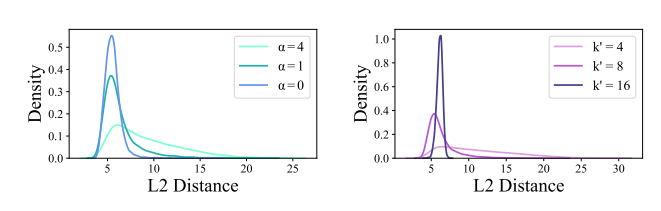


Fig. 16. l_2 -distance KDE on PreAct-ResNet18 trained by CIFAR-10 at 0.004% poisoning ratio (left) and 1% poisoning ratio (right).

Section III-Ec has demonstrated that models exhibit generalization ability. To confirm our conclusions, we conduct l_2 distance KDE visualization by modifying original information intensities α and trigger information intensities k' of the poisoned testing samples. Fig. 17(a) shows the l_2 -distance KDE visualization under different original information intensities α . With the increase of the intensity of original information α , the l_2 distance in feature space between the poisoned testing samples and the poisoned training samples gradually increases. As a result, the original information has a negative effect on the backdoor model, but we can rely on the model's generalization ability to activate the backdoor when the prominence of the trigger is stronger than that of the original information. Fig. 17(b) shows the l_2 -distance KDE visualization under different trigger information intensities k'. The increase of the trigger information intensity k' can promote the backdoor model to capture the trigger information, which is positive for the activation of the backdoor.



(a) l_2 -distance KDE under different (b) l_2 -distance KDE under different original information intensities α trigger information intensities k'

Fig. 17. l_2 -distance KDE on PreAct-ResNet18 trained by CIFAR-10 at 0.004% ratio.

VI. CONCLUSION

In this work, a novel frequency-based backdoor attack, WPDA, is proposed. By analyzing the frequency information distribution of datasets based on Wavelet Packet Decomposition (WPD), we infer the key frequency regions which the models would focus on and select the frequency regions to inject trigger. To promote the model to learn the trigger effectively, we conduct qualitative analyses experiments to design backdoor pattern. Our method not only remain the naturalness of backdoor samples, but also successfully achieve backdoor attack at extremely low poisoning ratios. Besides, we conduct t-SNE to analyze the distribution of the poisoned training samples and the poisoned testing samples in the feature space to vertify the effectiveness of our method. We also conduct l_2 -distance KDE visualization experiments to observe the l_2 -distance value of attacks at different poisoning ratios, demonstrating that WPDA prompts the model to efficiently learn the trigger information rather than memorizing the poisoned training samples at low poisoning ratios.

REFERENCES

- [1] N. Ahmed, T. Natarajan, and K. R. Rao, "Discrete cosine transform," *IEEE transactions on Computers*, 1974.
- [2] E. Bagdasaryan and V. Shmatikov, "Blind backdoors in deep learning models," in *USENIX Security Symposium*, 2021.
- [3] S. Balaban, "Deep learning and face recognition: the state of the art," Biometric and surveillance technology for human and activity identification XII, vol. 9457, pp. 68–75, 2015.

- [4] M. Barni, K. Kallas, and B. Tondi, "A new backdoor attack in cnns by training set corruption without label poisoning," in *International Conference on Image Processing*, 2019.
- [5] E. O. Brigham, The fast Fourier transform and its applications. Prentice-Hall, Inc., 1988.
- [6] B. Chen, W. Carvalho, N. Baracaldo, H. Ludwig, B. Edwards, T. Lee, I. Molloy, and B. Srivastava, "Detecting backdoor attacks on deep neural networks by activation clustering," arXiv preprint arXiv:1811.03728, 2018.
- [7] W. Chen, B. Wu, and H. Wang, "Effective backdoor defense by exploiting sensitivity of poisoned samples," in *Conference on Neural Information Processing Systems*, 2022.
- [8] X. Chen, C. Liu, B. Li, K. Lu, and D. Song, "Targeted backdoor attacks on deep learning systems using data poisoning," arXiv preprint arXiv:1712.05526, 2017.
- [9] S. Cheng, Y. Liu, S. Ma, and X. Zhang, "Deep feature space trojan attack of neural networks by controlled detoxification," in Association for the Advancement of Artificial Intelligence, 2021.
- [10] R. C. Damale and B. V. Pathak, "Face recognition based attendance system using machine learning algorithms," in 2018 Second International Conference on Intelligent Computing and Control Systems (ICICCS). IEEE, 2018, pp. 414–419.
- [11] J. Deng, W. Dong, R. Socher, L.-J. Li, K. Li, and L. Fei-Fei, "Imagenet: A large-scale hierarchical image database," in 2009 IEEE conference on computer vision and pattern recognition. Ieee, 2009, pp. 248–255.
- [12] K. Doan, Y. Lao, W. Zhao, and P. Li, "Lira: Learnable, imperceptible and robust backdoor attacks," in *Proceedings of the IEEE/CVF International Conference on Computer Vision*, 2021, pp. 11966–11976.
- [13] N. Dräger, Y. Xu, and P. Ghamisi, "Backdoor attacks for remote sensing data with wavelet transform. arxiv 2022," arXiv preprint arXiv:2211.08044, 2021.
- [14] Y. Feng, B. Ma, J. Zhang, S. Zhao, Y. Xia, and D. Tao, "Fiba: Frequency-injection based backdoor attack in medical image analysis," in *Conference on Computer Vision and Pattern Recognition*, 2022.
- [15] K. Gao, J. Bai, B. Wu, M. Ya, and S.-T. Xia, "Imperceptible and robust backdoor attack in 3d point cloud," *IEEE Transactions on Information Forensics and Security*, vol. 19, pp. 1267–1282, 2023.
- [16] Y. Gao, C. Xu, D. Wang, S. Chen, D. C. Ranasinghe, and S. Nepal, "Strip: A defence against trojan attacks on deep neural networks," in *Proceedings of the 35th Annual Computer Security Applications Conference*, 2019, pp. 113–125.
- [17] A. Gramacki, Nonparametric kernel density estimation and its computational aspects. Springer, 2018.
- [18] T. Gu, B. Dolan-Gavitt, and S. Garg, "Badnets: Identifying vulnerabilities in the machine learning model supply chain," arXiv preprint arXiv:1708.06733, 2019.
- [19] J. Guo, Y. Li, X. Chen, H. Guo, L. Sun, and C. Liu, "Scale-up: An efficient black-box input-level backdoor detection via analyzing scaled prediction consistency," in *International Conference on Learning Representations*, 2023.
- [20] J. Hayase, W. Kong, R. Somani, and S. Oh, "Spectre: Defending against backdoor attacks using robust statistics," in *International Conference on Machine Learning*, 2021.
- [21] K. He, X. Zhang, S. Ren, and J. Sun, "Identity mappings in deep residual networks," in *European conference on computer vision*. Springer, 2016, pp. 630–645.
- [22] K. Huang, Y. Li, B. Wu, Z. Qin, and K. Ren, "Backdoor defense via decoupling the training process," in *International Conference on Learning Representations*, 2022.
- [23] A. Krizhevsky and G. Hinton, "Learning multiple layers of features from tiny images," *Handbook of Systemic Autoimmune Diseases*, vol. 1, no. 4, 2009.
- [24] K. Kurita, P. Michel, and G. Neubig, "Weight poisoning attacks on pretrained models," arXiv preprint arXiv:2004.0660, 2020.
- [25] Y. Le and X. Yang, "Tiny imagenet visual recognition challenge," Convolutional Neural Networks for Visual Recognition, vol. 7, no. 7, p. 3, 2015.
- [26] J. Li, D. Yu, J.-T. Huang, and Y. Gong, "Improving wideband speech recognition using mixed-bandwidth training data in cd-dnn-hmm," in 2012 IEEE Spoken Language Technology Workshop (SLT), 2012.
- [27] Y. Li, X. Lyu, N. Koren, L. Lyu, B. Li, and X. Ma, "Anti-backdoor learning: Training clean models on poisoned data," in *Advances in Neural Information Processing Systems*, 2021.
- [28] —, "Neural attention distillation: Erasing backdoor triggers from deep neural networks," in *International Conference on Learning Representa*tions, 2021.

- [29] Y. Li, Y. Li, B. Wu, L. Li, R. He, and S. Lyu, "Invisible backdoor attack with sample-specific triggers," in *Proceedings of the IEEE/CVF International Conference on Computer Vision*, 2021, pp. 16463–16472.
- [30] X. Liu, M. Li, H. Wang, S. Hu, D. Ye, H. Jin, L. Wu, and C. Xiao, "Detecting backdoors during the inference stage based on corruption robustness consistency," in *Conference on Computer Vision and Pattern Recognition*, 2023.
- [31] W. Ma, D. Wang, R. Sun, M. Xue, S. Wen, and Y. Xiang, "The "beatrix" resurrections: Robust backdoor detection via gram matrices," in *Network and Distributed System Security Symposium*, 2023.
- [32] T. A. Nguyen and A. Tran, "Input-aware dynamic backdoor attack," in Advances in Neural Information Processing Systems, 2020.
- [33] T. A. Nguyen and A. T. Tran, "Wanet imperceptible warping-based backdoor attack," in *International Conference on Learning Representa*tions, 2021.
- [34] R. Ning, J. Li, C. Xin, and H. Wu, "Invisible poison: A blackbox clean label backdoor attack to deep neural networks," in *IEEE Conference on Computer Communications*, 2021.
- [35] M. Pan, Y. Zeng, L. Lyu, X. Lin, and R. Jia, "ASSET: robust backdoor data detection across a multiplicity of deep learning paradigms," in USENIX Security Symposium, 2023.
- [36] X. Qi, T. Xie, T. Wang, T. Wu, S. Mahloujifar, and P. Mittal, "Towards a proactive ml approach for detecting backdoor poison samples," in USENIX Security Symposium, 2023.
- [37] A. Shafahi, W. R. Huang, M. Najibi, O. Suciu, C. Studer, T. Dumitras, and T. Goldstein, "Poison frogs! targeted clean-label poisoning attacks on neural networks," in *Advances in Neural Information Processing* Systems, 2018.
- [38] I. Shumailov, Z. Shumaylov, D. Kazhdan, Y. Zhao, N. Papernot, M. A. Erdogdu, and R. J. Anderson, "Manipulating sgd with data ordering attacks," in Advances in Neural Information Processing Systems, 2021.
- [39] K. Simonyan and A. Zisserman, "Very deep convolutional networks for large-scale image recognition," in 3rd International Conference on Learning Representations, 2015.
- [40] H. Souri, L. Fowl, R. Chellappa, M. Goldblum, and T. Goldstein, "Sleeper agent: Scalable hidden trigger backdoors for neural networks trained from scratch," Advances in Neural Information Processing Systems, vol. 35, pp. 19165–19178, 2022.
- [41] W. Sun, X. Jiang, S. Dou, D. Li, D. Miao, C. Deng, and C. Zhao, "Invisible backdoor attack with dynamic triggers against person reidentification," *Transactions on Information Forensics and Security*, vol. 19, pp. 307–319, 2024.
- [42] D. Tang, X. Wang, H. Tang, and K. Zhang, "Demon in the variant: Statistical analysis of {DNNs} for robust backdoor contamination detection," in USENIX Security Symposium, 2021.
- [43] Y. Tian, F. Suya, F. Xu, and D. Evans, "Stealthy backdoors as compression artifacts," *Transactions on Information Forensics and Security*, vol. 17, pp. 1372–1387, 2022.
- [44] B. Tran, J. Li, and A. Madry, "Spectral signatures in backdoor attacks," in Advances in Neural Information Processing Systems Workshop, 2018.
- [45] B. Wang, Y. Yao, S. Shan, H. Li, B. Viswanath, H. Zheng, and B. Y. Zhao, "Neural cleanse: Identifying and mitigating backdoor attacks in neural networks," in 2019 IEEE Symposium on Security and Privacy (SP), 2019.
- [46] T. Wang, Y. Yao, F. Xu, S. An, H. Tong, and T. Wang, "An invisible black-box backdoor attack through frequency domain," in *European Conference on Computer Vision*, 2022.
- [47] Y. Wang, M. Zhao, S. Li, X. Yuan, and W. Ni, "Dispersed pixel perturbation-based imperceptible backdoor trigger for image classifier models," *Transactions on Information Forensics and Security*, vol. 17, pp. 3091–3106, 2022.
- [48] S. Wei, M. Zhang, H. Zha, and B. Wu, "Shared adversarial unlearning: Backdoor mitigation by unlearning shared adversarial examples," in Thirty-seventh Conference on Neural Information Processing Systems, 2023.
- [49] S. Winograd, "On computing the discrete fourier transform," Mathematics of computation, 1978.
- [50] B. Wu, H. Chen, M. Zhang, Z. Zhu, S. Wei, D. Yuan, and C. Shen, "Backdoorbench: A comprehensive benchmark of backdoor learning," in Conference on Neural Information Processing Systems Datasets and Benchmarks Track, 2022.
- [51] B. Wu, H. Chen, M. Zhang, Z. Zhu, S. Wei, D. Yuan, C. Shen, and H. Zha, "Backdoorbench: A comprehensive benchmark of backdoor learning," in *Conference on Neural Information Processing Systems*, 2022.

- [52] B. Wu, S. Wei, M. Zhu, M. Zheng, Z. Zhu, M. Zhang, H. Chen, D. Yuan, L. Liu, and Q. Liu, "Defenses in adversarial machine learning: A survey," arXiv preprint arXiv:2312.08890, 2023.
- [53] D. Wu and Y. Wang, "Adversarial neuron pruning purifies backdoored deep models," in Advances in Neural Information Processing Systems, 2021.
- [54] Z. Xiong, K. Ramchandran, and M. T. Orchard, "Wavelet packet image coding using space-frequency quantization," *Transactions on Image Processing*, vol. 7, no. 6, pp. 892–898, 1998.
- [55] D. Yuan, S. Wei, M. Zhang, L. Liu, and B. Wu, "Activation gradient based poisoned sample detection against backdoor attacks," arXiv preprint arXiv:2312.06230, 2023.
- [56] X. Yuan, Y. Chen, Y. Zhao, Y. Long, X. Liu, K. Chen, S. Zhang, H. Huang, X. Wang, and C. A. Gunter, "Commandersong: A systematic approach for practical adversarial voice recognition," in 27th {USENIX} Security Symposium ({USENIX} Security 18), 2018.
- [57] Y. Zeng, S. Chen, W. Park, Z. Mao, M. Jin, and R. Jia, "Adversarial unlearning of backdoors via implicit hypergradient," in *International Conference on Learning Representations*, 2022.
- [58] Y. Zeng, W. Park, Z. M. Mao, and R. Jia, "Rethinking the backdoor attacks' triggers: A frequency perspective," in *International Conference* on Computer Vision, 2021.
- [59] Q. Zhang, Y. Ding, Y. Tian, J. Guo, M. Yuan, and Y. Jiang, "Advdoor: adversarial backdoor attack of deep learning system," in *Proceedings of the 30th ACM SIGSOFT International Symposium on Software Testing and Analysis*, 2021.
- [60] S. Zhao, X. Ma, X. Zheng, J. Bailey, J. Chen, and Y.-G. Jiang, "Clean-label backdoor attacks on video recognition models," in *Proceedings of the IEEE/CVF Conference on Computer Vision and Pattern Recognition*, 2020.
- [61] R. Zheng, R. Tang, J. Li, and L. Liu, "Data-free backdoor removal based on channel lipschitzness," in *European Conference on Computer Vision*, 2022.
- [62] H. Zhou, W. Li, Z. Kong, J. Guo, Y. Zhang, B. Yu, L. Zhang, and C. Liu, "Deepbillboard: Systematic physical-world testing of autonomous driving systems," in *Proceedings of the ACM/IEEE 42nd International Conference on Software Engineering*, 2020.
- [63] M. Zhu, S. Wei, H. Zha, and B. Wu, "Neural polarizer: A lightweight and effective backdoor defense via purifying poisoned features," arXiv preprint arXiv:2306.16697, 2023.